

# Electrocatalytic Nitrate Reduction to Ammonia: From Microscopic Reaction Kinetics to Advanced Catalyst Design Strategies

---

Date of Submission: 09-04-2026

Date of Acceptance: 22-04-2026

---

## I. Introduction and Industrial Background

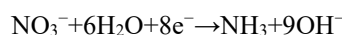
Nitrogen is the fundamental cornerstone of life and the Earth's ecosystem. Its fixation, nitrification, and denitrification processes in nature constitute the crucial ecological nitrogen cycle[1]. However, since the invention of the Haber-Bosch process, humanity has dramatically interfered with the natural cycle through high-temperature, high-pressure industrial nitrogen fixation to meet the enormous demand for agricultural fertilizers[2]. It is estimated that approximately 48% of the global population relies on artificially synthesized nitrogen fertilizers for food production. This not only consumes over 1% of the world's energy supply but also contributes to more than 1% of global carbon dioxide emissions[3].

More critically, the excessive application of synthetic nitrogen fertilizers, nitrogen-containing industrial wastewater from mining activities, and nitrogen oxides (NO<sub>x</sub>) emitted from transportation eventually permeate water bodies and are converted into nitrate (NO<sub>3</sub><sup>-</sup>), which exhibits high chemical stability and high water solubility[4]. The massive accumulation of nitrate not only leads to widespread eutrophication in aquatic ecosystems but also poses a direct threat to human health. Once nitrate enters the human body through drinking water, it can readily cause fatal infant methemoglobinemia (oxidizing hemoglobin to methemoglobin, which loses its oxygen-carrying capacity)[5]. Furthermore, in the human stomach, nitrite intermediates can easily react with nitrosatable compounds to form strongly carcinogenic N-nitroso compounds.

For the modern environmental protection and chemical industries, traditional physical denitrification technologies such as reverse osmosis[6], ion exchange, electro dialysis[7], or capacitive deionization[8] merely achieve the "spatial transfer" of pollutants. The resulting nitrate-rich concentrated waste liquid still poses a challenge for secondary treatment. Against this macro background, the **electrocatalytic nitrate reduction reaction (NO<sub>3</sub>RR)** emerges as a green-electricity-driven technology operating under ambient temperature and pressure. It can not only fundamentally eliminate the toxicity in water bodies but also directly convert this nitrogenous "waste" into high-value-added ammonia (NH<sub>3</sub>). Ammonia is not only a fundamental raw material for the modern chemical industry but is also regarded as a highly promising zero-carbon liquid fuel and hydrogen energy storage/transport carrier due to its high mass hydrogen storage density of 17.7 wt% and volumetric energy density of 108 g L<sup>-1</sup>(at 20°C and 857 kPa)[9]. Therefore, gaining a deep understanding of the catalytic mechanisms of NO<sub>3</sub>RR and developing efficient electrocatalytic materials has become a core bridge connecting "environmental remediation" and "new energy conversion"[10].

## II. Thermodynamic and kinetic mechanisms of electrocatalytic nitrate reduction to ammonia

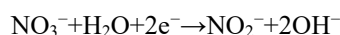
The complete reduction of NO<sub>3</sub><sup>-</sup> to NH<sub>3</sub> is an extremely complex process involving the grand engineering of eight-electron (8e<sup>-</sup>) coupling and nine-proton transfer. Its overall reaction equation in an aqueous electrolyte is as follows:



From the perspective of electrochemical reaction kinetics, the microscopic evolution of this reaction on the catalyst surface is primarily dissected into two core stages: the initial deoxygenation stage and the subsequent deep hydrogenation stage.

### 2.1 Initial Deoxygenation: Breaking the Energy Barrier of the Rate Determining Step

The starting point of the reaction is the adsorption of the nitrate ion molecule at the catalyst interface and the initial electron injection.



Kinetic measurements indicate that on copper-based electrodes in sulfuric acid solution, the Tafel slope for this step is approximately 130 mV dec<sup>-1</sup> (close to the theoretical 128 mV dec<sup>-1</sup> for single-electron transfer control)[11]. This data, along with transient radiation decomposition and photoelectron emission studies,

confirms that hydrated electrons first combine with  $\text{NO}_3^-$  to generate the high-energy  $\text{NO}_3^-$  radical[12]. Due to the highly symmetric planar resonance structure ( $D_{3h}$ ) of the  $\text{NO}_3^-$  molecule, its lowest unoccupied molecular orbital (LUMO) energy level is extremely high, presenting a significant thermodynamic barrier to electron injection[13]. Once this barrier is overcome, the highly oxidizing  $\text{NO}_3^-$  instantly undergoes deoxygenation and collapses, converting to  $^*\text{NO}_2^-$  or adsorbed  $^*\text{NO}_2$ . Therefore, this deoxygenation process is widely recognized in academia as the rate-determining step (RDS) for the entire  $\text{NO}_3^-$ RR[14].

## 2.2 Deep Hydrogenation: Complex Branching Networks

As  $^*\text{NO}_2^-$  further receives electrons (at approximately  $-0.47$  V vs. SHE) and is deoxygenated to form the key intermediate  $^*\text{NO}$ , the reaction officially enters the hydrogenation stage, which is highly governed by the coverage of surface hydrogen species ( $^*\text{H}$ ). Based on monitoring by infrared spectroscopy and differential electrochemical mass spectrometry (DEMS), the academic community has proposed three mainstream parallel and competitive pathways[15]:

**Hydrogenation-First, Then Deoxygenation Pathway:** The nitrogen atom is preferentially protonated ( $^*\text{NO} \rightarrow ^*\text{HNOH}$ ), followed by the removal of the coordinated oxygen atom, generating a hydroxylamine intermediate ( $^*\text{HNOH} \rightarrow ^*\text{NH}_2\text{OH} \rightarrow ^*\text{NH}_3$ ).

**Complete Deoxygenation Followed by Sequential Hydrogenation Pathway:** The N-O bond in  $^*\text{NO}$  directly breaks, stripping off the oxygen atom ( $^*\text{NO} \rightarrow ^*\text{N}$ ). Subsequently, the exposed nitrogen atom undergoes three consecutive hydrogenation steps ( $^*\text{N} \rightarrow ^*\text{NH} \rightarrow ^*\text{NH}_2 \rightarrow ^*\text{NH}_3$ ).

**Alternating Hydrogenation-Deoxygenation Pathway:** After protonation forms  $^*\text{HNOH}$ , the non-coordinated oxygen undergoes stepwise deoxygenation reduction.

Furthermore, the N-N coupling side reaction frequently observed in isotope and spectroscopic experiments cannot be ignored[16]. When the concentration of  $^*\text{NH}$  species on the catalyst surface is too high or their binding energy is too strong, bimolecular coupling readily occurs, generating  $\text{N}_2\text{H}_4$  analogs or directly releasing nitrogen gas ( $\text{N}_2$ ). The ultimate revelation for industrial R&D is: an efficient ammonia synthesis catalyst must achieve an extremely delicate kinetic balance between "anchoring intermediates to prevent  $\text{NO}_2^-$  loss" and "precisely controlling the surface hydrogen evolution reaction (HER) to provide just the right amount of localized active hydrogen"[17].

## III. Standardized and Anti-Interference Product Analysis Qualitative and Quantitative System

When evaluating the real performance of electrocatalytic materials, eliminating false positives (such as ammonia contamination from the air, degradation of nitrogen-containing polymer binders) and achieving precise quantification of products at extremely low concentrations are the primary engineering challenges faced by both industry and academia.

For the target product, ammonia (which typically exists as  $\text{NH}_3$  or  $\text{NH}_4^+$  in the system due to acid-base equilibrium), the most mainstream and lowest-cost method currently is ultraviolet-visible (UV-vis) spectrophotometric colorimetry. However, it is internally divided into two major schools with distinctly different applicable scenarios[18]:

**Indophenol Blue (IB) Method:** Based on the Berthelot reagent reaction. Ammonia in the water sample, catalyzed by sodium nitroferricyanide ( $[\text{Fe}(\text{CN})_5\text{NO}]^{2-}$ ), reacts with phenol and hypochlorite ( $\text{ClO}^-$ ) to form a deep-blue indophenol compound, which has a maximum absorption peak at 655 nm. This method exhibits excellent linearity within the concentration range of 0-2000  $\mu\text{g L}^{-1}$ . However, the biggest pitfall in industrial testing is its pH sensitivity: hypochlorite is extremely unstable in acidic media. Studies show that if a pH=4 electrolyte is directly subjected to the color development, the negative deviation of the measured concentration can be as high as -75.6%. Pre-neutralization with alkali is essential to ensure data validity.

**Nessler's Reagent (NR) Method:** Uses a strongly alkaline solution of potassium tetraiodomercurate(II) ( $\text{K}_2\text{HgI}_4$ ) as the chromogenic agent. The tetraiodomercurate anion in the system reacts with ammonia to form a reddish-brown  $\text{Hg}_2\text{ONH}_2\text{I}$  complex, with an absorption peak at 420 nm. Compared to the IB method, the NR method exhibits strong robustness against pH fluctuations, with errors controlled within -11% even without pH adjustment, making it the preferred engineering testing scheme for acidic electrolytes[19].

Detection of byproducts and reactants also requires standardization: Nitrate ( $\text{NO}_3^-$ ) can usually be directly quantified by reading the absorption peak in the deep ultraviolet region at 220 nm. In contrast, the quantification of the key intermediate, nitrite ( $\text{NO}_2^-$ ), heavily relies on the Griess reagent. Sulfanilamide reacts with nitrite under acidic conditions to form a diazonium salt, which subsequently undergoes a diazo coupling reaction with N-(1-naphthyl)-ethylenediamine dihydrochloride, forming a characteristic azo dye for quantification at 540 nm[20].

To definitively confirm the true source of ammonia, isotope-labeled Nuclear Magnetic Resonance ( $^1\text{H}$  NMR) spectroscopy serves as the conclusive "smoking gun" evidence. Due to the fundamental difference in nuclear spin quantum numbers, when the isotopically labeled  $^{15}\text{NO}_3^-$  is used as the reaction substrate instead of

naturally abundant  $^{14}\text{NO}_3^-$ , the product  $^{15}\text{NH}_4^+$  produces a characteristic doublet resonance split at 7.15 ppm, whereas the background  $^{14}\text{NH}_4^+$  exhibits a distinct triplet.

#### **IV. Nitrate-to-Ammonia Electrocatalyst Materials and Advanced Design Strategies**

##### **4.1 Metal electrodes: Finding the extrema of a volcano plot**

Early studies employed microkinetic modeling to construct a global thermodynamic volcano plot, establishing that a metal's adsorption energy for oxygen ( $\Delta\text{EO}$ ) and nitrogen ( $\Delta\text{EN}$ ) is the core "descriptor" for predicting product selectivity[21]. For example, the d-orbitals of iron (Fe) and cobalt (Co) bind nitrogen species too strongly, making desorption difficult and leading to frequent surface collisions and coupling between intermediates, thereby steering the system towards the dead end of  $\text{N}_2$  generation. Conversely, the adsorption energies of gold (Au) and silver (Ag) are too weak, causing intermediates to desorb immediately after deoxygenation, resulting in products dominated by toxic NO and  $\text{NO}_2^-$ . Theoretically, metals like copper (Cu) and rhodium (Rh) reside in the intermediate "golden zone" of adsorption energy, making them the most promising candidates for highly selective ammonia synthesis[22].

However, a formidable chasm for industrial-grade application is the competing hydrogen evolution reaction (HER). For traditional precious HER metals like platinum (Pt), palladium (Pd), and ruthenium (Ru), a slight negative potential ( $< 0$  V vs. RHE) triggers severe hydrogen underpotential deposition (HUPD)[23]. A high density of surface-adsorbed hydrogen ( $^*\text{H}$ ) forms a dense, armor-like layer covering facets like Pt(110), directly blocking the access of nitrate ions ( $\text{NO}_3^-$ ) from the bulk solution to the active metal sites[24]. Even with finely controlled morphologies, such as synthesized one-dimensional iridium nanotubes (Ir NTs) electrodes, which barely achieved a Faradaic efficiency of 84.7% for ammonia production at a slightly positive potential of 0.06 V, once the operating potential dropped below 0 V, the ammonia production efficiency plummeted dramatically below 25% alongside vigorous bubble generation[25]. This indicates that pure precious metals are ill-suited for industrial high-current-density reductive conditions[26]. Modifying the Pt surface with heterogeneous atoms like Rh, Cu, Sn, or Ge, while leveraging bifunctional synergy (heteroatoms capture and deoxygenate nitrate, Pt handles hydrogenation), still cannot fundamentally eliminate the constraint imposed by HER[27, 28]. In recent years, oxide-derived silver (Oxide-derived Ag) has shown potential in suppressing HER, but its efficiency for complete conversion to ammonia still needs improvement[29, 30].

##### **4.2 Crystal Face Dependence: The Magic of Atomic Arrangement**

In copper-based non-precious metal systems with high intrinsic activity, the spatial arrangement of surface atoms (crystal facets) becomes the "steering wheel" dominating the microscopic reaction pathway[31].

Kang's team meticulously designed a set of comparative experiments, preparing Cu nanoparticles with no specific facets, Cu nanocubes exposing regular {100} facets, and Cu nanosheets (CuNSs) dominated by extensive {111} basal planes[32]. Linear sweep voltammetry (LSV) and potentiostatic electrolysis tests revealed a striking result: at an extremely mild bias (-0.15 V vs. RHE), CuNSs achieved an astonishing Faradaic efficiency for ammonia production of 99.7%, far surpassing the other morphologies.

Deciphering the underlying microscopic mechanism relied on the combined application of in situ shell-isolated nanoparticle-enhanced Raman spectroscopy (SHINERS) and electrochemical scanning tunneling microscopy (EC-STM)[33]. Studies confirmed that within the  $\text{NO}_3\text{RR}$  potential window, compared to the densely packed Cu(100), the Cu(111) facet has a lower thermodynamic surface energy and is extremely prone to spontaneously adsorbing free oxygen to form an ultra-thin surface oxide layer ( $\text{Cu}_2\text{O}$ )[34]. This oxidation process perfectly aligns with the reaction's rate-determining step: the nitrate molecule "transfers" an oxygen atom to the Cu(111) facet to form cuprous oxide, while itself successfully completes the first deoxygenation step, degrading to nitrite.

In palladium (Pd)-based materials, this "facet division of labor" is even more intriguing. Hatzell et al. synthesized palladium cuboctahedra containing both {100} and {111} facets, whose ammonia production activity surpassed that of single-faceted pure octahedra and cubes[35]. In-depth investigation revealed: the {111} facets act as specialized "breachers," responsible only for reducing  $\text{NO}_3^-$  to  $\text{NO}_2^-$ ; while the {100} facets serve as efficient "hydrogenation stations," taking over to convert  $\text{NO}_2^-$  into ammonia. This demonstrates that designing catalysts with controlled morphology to achieve multi-facet cooperation is a crucial direction for industrial scale-up.

##### **4.3 Doping, Alloying, and Strain Engineering: Manipulating Electronic Energy Bands**

When conventional morphology control reaches its limits, the electronic perturbation induced by forcibly embedding heteroatoms into the crystal lattice becomes a key technique for modulating the adsorption energy of intermediates.

Interfacial Charge Transfer Effect: Zhang et al. successfully utilized the work function difference at the metal oxide/pure metal interface in electrochemically in-situ reconstructed Cu/Cu<sub>2</sub>O nanowire arrays. Electrons

spontaneously flow from Cu<sub>2</sub>O to pure Cu across the heterojunction, resulting in a state of localized high electron cloud density on the surface Cu[36]. Density functional theory (DFT) calculations show that these electron-rich Cu sites significantly stabilize the \*NOH intermediate, which is highly prone to dissociation during hydrogenation, ultimately boosting the ammonia selectivity to 81.2% and achieving a remarkable production rate of 0.2449 mmol h<sup>-1</sup>cm<sup>-2</sup>. Similarly, in the Ni<sub>3</sub>B@NiB<sub>2.74</sub> core-shell structure, the introduced boron (B) atoms, utilizing their unoccupied valence 2p orbitals, act as strong Lewis acid sites. They precisely anchor and activate the nitrate ion, which acts as a Lewis base, through acid-base interactions[37].

**Strain Engineering:** Lattice distortion often harbors the power to alter catalytic destiny[38, 39]. Researchers introduced a tensile strain as high as 12% between surface Ru atoms by precisely doping oxygen into the subsurface of ruthenium (Ru) nanoclusters. This subtle lattice stretching ingeniously increases the energy barrier for the Heyrovsky step (\*H+H<sub>3</sub>O<sup>++</sup>e<sup>-</sup>→H<sub>2</sub>+H<sub>2</sub>O) of hydrogen atoms on the surface, forcibly suppressing H-H coupling and hydrogen gas evolution. Consequently, a large number of free, highly reactive single-atom \*H species are "forced" to participate in the deep hydrogenation processes of \*HNO and \*NH<sub>2</sub>. At a bias of 0.8 V, the partial current density for ammonia production in this strained structure increased by 77 times compared to the ordinary structure.

**d-Band Center Shift (d-Band Theory):** The Cu<sub>50</sub>Ni<sub>50</sub> bimetallic alloy developed by Sargent's group is a classic example of band engineering[40]. Pure Cu suffers from relatively weak adsorption of the initial \*NO<sub>3</sub> due to its deep d-band center, which becomes a bottleneck limiting its activity. After introducing Ni to form the alloy, the overall d-band center of the system shifts upward towards the Fermi level. This indicates fewer antibonding orbitals are occupied, greatly enhancing the surface's ability to capture reaction substrates. In computational models, the maximum free energy barrier for the first step of nitrate adsorption on the Cu<sub>50</sub>Ni<sub>50</sub> surface decreases sharply, enabling it to achieve an industrial-grade current density of 100 mA cm<sup>-2</sup> with 99% Faradaic efficiency for ammonia at an ultralow overpotential of just -0.05 V (vs. RHE).

#### **4.4 Single-atom catalysts (SACs): From nano to sub-nano limits**

To push the atomic utilization of metals to the 100% limit and establish uniformly distributed coordination-active centers, single-atom catalyst (SAC) technology has fundamentally reshaped the research paradigm in this field in recent years[41].

Isolated copper atoms anchored on the organic semiconductor macromolecule PTCDA (3,4,9,10-perylenetetracarboxylic dianhydride), denoted as Cu-PTCDA, have demonstrated unparalleled dominance, surpassing metals like bismuth, iridium, cobalt, and nickel[42]. Delving into the essence of its electronic orbitals: the isolated Cu atom maintains a fully occupied 3d<sup>10</sup> electron configuration. When a nitrate ion approaches, its highest occupied molecular orbital (HOMO) forms a bond with the empty orbitals of Cu, while at the same time, the electron-rich 3d electrons of Cu are forcefully injected into the antibonding LUMO orbital of nitrate, forming an extremely stable "back-bonding" interaction. Projected density of states (PDOS) analysis confirms deep energy-level hybridization between the O 2p and Cu 3d orbitals. This "death-grip" like anchoring directly contributes to an ultimate production rate of 436 μg h<sup>-1</sup>cm<sup>-2</sup>. Similarly, Cu-N-C, with copper anchored on nitrogen-doped carbon supports, shines brilliantly. Its unique Cu(I)-N<sub>2</sub> and Cu(II)-N<sub>4</sub> configurations tenaciously lock onto the toxic intermediate \*NO<sub>2</sub>—produced during the reduction, achieving a direct eight-electron reduction from NO<sub>3</sub><sup>-</sup> to NH<sub>3</sub> in one continuous process, thoroughly eliminating the risk of nitrite leakage into water bodies[43].

Beyond copper, single-atom iron also shows remarkable potential. Using in-situ surface interrogation via scanning electrochemical microscopy (SI-SECM), scientists observed the astounding "site-occupying effect" of the Fe(II)-N<sub>x</sub> coordination center in Fe-PPy catalysts[44]. Even at elevated bias and in solutions with high proton concentration, nitrate ions, with their substantial thermodynamic advantage, preferentially and firmly occupy the Fe(II) sites[45]. Since protons are deprived of any opportunity to approach the iron atoms, the competing HER reaction is kinetically "strangled in the cradle." Furthermore, theoretical calculations prospectively indicate that titanium and zirconium supported on graphitic carbon nitride (Ti/g-CN, Zr/g-CN) have limiting potentials as low as -0.39 V and -0.41 V, respectively, with potential even surpassing that of Cu single-atom catalysts. This provides a theoretical compass for matching next-generation ideal supports with active metals[46].

#### **4.5 Defect Engineering of Metal Oxides: The 'Clamp Attack' of Oxygen Vacancies**

Compared to pure metals, cost-effective transition metal oxides (such as TiO<sub>2</sub>, CuO) gain top-tier electrocatalytic activity through artificially creating surface oxygen vacancies (OVs) by methods like plasma bombardment or high-temperature reduction gas treatment, which strip lattice oxygen.

In TiO<sub>2</sub>-x materials obtained via high-temperature hydrogen treatment, surface OVs act as excellent chemisorption traps[47]. DFT simulations depict a vivid microscopic scene: on a TiO<sub>2</sub>(101) facet with two consecutive oxygen vacancies, the nitrate ion not only anchors itself by occupying a pre-existing vacancy but

also forms a new Ti-O bond with an adjacent unsaturated Ti atom through its other oxygen atom. This dual-site cooperative "pincer configuration" dramatically lowers the free energy step for the entire deoxygenation reaction. Concurrently, due to the presence of lattice defects, excess 3d electrons from Ti transition and occupy states at the bottom of the conduction band, endowing the material with near-metallic excellent conductivity. This ultimately resulted in a high selectivity of 87.1% in experiments.

Based on the same philosophy, defect-engineered CuO<sub>2-x</sub>, prepared by flame spray pyrolysis followed by helium plasma etching, achieved an orders-of-magnitude leap in NH<sub>4</sub><sup>+</sup> production rate (peak near 300 μmol cm<sup>-2</sup>h<sup>-1</sup>) compared to defect-free pristine CuO. This once again verifies the universal industrial principle of vacancy-dominated catalytic pathways[48].

#### **4.6 Bionic Molecular-Level Assembly: Borrowing Answers from Nature**

Although the development of artificial materials progresses rapidly, efficient denitrification under neutral and mild conditions (the environment of most natural water bodies) remains a tough nut to crack. Most metallic materials require an extremely harsh, strongly acidic environment (pH<1) to promote the protonation of NO<sub>3</sub><sup>-</sup> (forming the more readily activated HNO<sub>3</sub>, pK<sub>a</sub>=-1.3). However, the nitrate reductase (NRase) found in nature thrives effortlessly under physiological neutral conditions.

Unveiling the mystery of this biocatalyst reveals that its active center is a Mo-S catalytic site, consisting of a mononuclear molybdenum (Mo) atom coordinated with surrounding oxo and dithiolene sulfur ligands. Inspired by this, chemists synthesized a highly biomimetic amorphous oxo-molybdenum sulfide structure (oxo-MoS<sub>x</sub>) using molybdate and L-cysteine as precursors via a hydrothermal method[49].

This represents an epic breakthrough in biomimicry. Through comprehensive tracking with electron paramagnetic resonance (EPR) and in situ Raman spectroscopy, the research team captured the fleeting MoV=O active species during the reaction. One oxygen atom of the nitrate ion can overlap very precisely with the 4d<sub>xy</sub> orbital of the MoV center. This configuration is energetically far more favorable than exciting the traditional π\* orbitals, facilitating an exceptionally efficient "proton-coupled electron transfer (PCET)" process. In comparative tests, highly crystalline conventional MoS<sub>2</sub> (lacking the crucial Mo=O defect configuration) exhibited a Faradaic efficiency of less than 5%, whereas the biomimetic oxo-MoS<sub>x</sub> material maintained a dominant Faradaic efficiency for ammonia production exceeding 96% even at 0 V bias in a completely neutral pH=7 buffer. Its reaction conversion rate was 18.8 times higher than that of the former. This provides the ultimate blueprint for developing the next generation of green, acid-waste-free distributed water treatment devices.

### **V. Summary and Industrialization Panorama Outlook**

In summary, systematic innovation across multiple dimensions—including nanostructuring, crystal facet engineering, alloying, lattice strain, defect engineering, single-atom catalysis, and biomimetic coordination—enables the electrocatalytic nitrate reduction reaction to ammonia (NO<sub>3</sub>RR) to not only address a grand environmental crisis but also reveal a compelling prospect for disrupting the century-old Haber-Bosch ammonia synthesis route. The highly efficient catalysts capable of being scaled to industrial levels of thousands of tons in the future must, in their microscopic design, balance four key engineering principles: Maximally Enhancing Deoxygenation Kinetics: Embrace easily oxidizable crystal facets or artificially create oxygen vacancy defects to break the initial rate-determining barrier. Precisely Tuning the d-band Center to Lock Intermediates: Utilize alloying or single-atom orbital hybridization to ensure nitrate and highly toxic intermediate phases like \*NO<sub>2</sub> do not desorb and escape prematurely.

Accurately Managing Hydrogen Supply: Suppress H-H coupling and hydrogen gas evolution via methods like strain engineering, preserving sufficient protons and atomic \*H for deep N-H bond formation.

Perspectives Towards Future Chemical Industry Architecture: While current research on the intrinsic activity of materials is approaching its pinnacle, the constraints of microfluidic mass transport become apparent during device-level scaling. Within porous electrodes or three-dimensional frameworks, the limited diffusion of reactants and the accumulation of concentrated ammonia products on the surface can severely poison active sites. Therefore, employing rotating disk electrodes (RDEs) to eliminate concentration polarization, combined with hydrodynamic simulations to optimize the design of continuous-flow reactors, represents the final step in bridging the gap between the laboratory and the factory.

An even more inspiring grand vision is the concept of a "Closed Carbon-Nitrogen Cycle Ecosystem." Standalone NO<sub>3</sub>RR can only treat wastewater. However, in a future zero-carbon super-electrolyzer system, we could couple it at the anode with a direct electrocatalytic dinitrogen oxidation reaction, continuously converting air into NO<sub>3</sub><sup>-</sup> to feed the cathode. Going a step further, by employing bifunctional alloy catalysts like tellurium-doped palladium (Te-Pd NCs) at the cathode, the nucleophilic \*CO intermediate generated from the CO<sub>2</sub> reduction reaction (CO<sub>2</sub>RR) could be forcibly coupled in situ with the highly reactive nitrogenous intermediates from NO<sub>3</sub>RR, driving carbon-nitrogen (C-N) coupling[50]. Then, humanity could potentially use a single integrated device to "consume" air and carbon dioxide on one end and directly "produce" high-value

fertilizers like urea or industrial solvents like acetamide on the other. This revolution in reaction engineering, driven by microscopic electronic orbitals, is destined to reshape the future map of Earth's resource cycles.

## References

- [1] Ryu, M. H.; Zhang, J.; Toth, T.; et al. Control of nitrogen fixation in bacteria that associate with cereals. *Nat. Microbiol.*, **2020**, *5*, 314-330.
- [2] Erisman, J. W.; Sutton, M. A.; Galloway, J.; Klimont, Z.; Winiwarter, W. How a century of ammonia synthesis changed the world. *Nat. Geosci.*, **2008**, *1*, 636-639.
- [3] Wood, S.; Cowie, A. A review of greenhouse gas emission factors for fertiliser production. *Climate technology center & network*, **2004**, Copenhagen.
- [4] Kuypers, M. M. M.; Marchant, H. K.; Kartal, B. The microbial nitrogen-cycling network. *Nat. Rev. Microbiol.*, **2018**, *16*, 263-276.
- [5] Speijers, G. J. A. Nitrate and nitrite in drinking-water, background document for development of WHO guidelines for drinking-water quality. *World Health Organization Press*, **2011**, Geneva.
- [6] Epsztein, R.; Nir, O.; Lahav, O.; Green, M. Selective nitrate removal from groundwater using a hybrid nanofiltration-reverse osmosis filtration scheme. *Chem. Eng. J.*, **2015**, *279*, 372-378.
- [7] Elmidaoui, A.; Menkouchi Sahli, M. A.; et al. Selective nitrate removal by coupling electrodialysis and a bioreactor. *Desalination*, **2002**, *153*, 389-397.
- [8] Qu, Y.; Campbell, P. G.; et al. Charging and Transport Dynamics of a Flow-Through Electrode Capacitive Deionization System. *J. Phys. Chem. B*, **2018**, *122*, 240-249.
- [9] Lamb, K. E.; Dolan, M. D.; Kennedy, D. F. Ammonia for hydrogen storage; A review of catalytic ammonia decomposition and hydrogen separation and purification. *Int. J. Hydrogen Energy*, **2019**, *44*, 3580-3593.
- [10] Choi, J.; Suryanto, B. H. R.; Wang, D.; et al. Identification and elimination of false positives in electrochemical nitrogen reduction studies. *Nat. Commun.*, **2020**, *11*, 5546.
- [11] Zeng, Y.; Priest, C.; Wang, G.; Wu, G. Restoring the Nitrogen Cycle by Electrochemical Reduction of Nitrate: Progress and Prospects. *Small Methods*, **2020**, *4*, 2000672.
- [12] Cook, A. R.; Dimitrijevic, N.; et al. Reducing radicals in nitrate solution. The  $\text{NO}_3^-$  system revisited. *J. Phys. Chem. A*, **2001**, *105*, 3658-3666.
- [13] da Cunha, M. C. P. M.; Weber, M.; Nart, F. C. On the adsorption and reduction of  $\text{NO}_3^-$  ions at Au and Pt electrodes studied by in situ FTIR spectroscopy. *J. Electroanal. Chem.*, **1996**, *414*, 163-170.
- [14] Zhang, Z.; Shi, W.; Wang, W.; et al. Interfacial electronic effects of palladium nanocatalysts on the by-product ammonia selectivity during nitrite catalytic reduction. *Environ. Sci.: Nano*, **2018**, *5*, 338-349.
- [15] Wang, Y.; Zhou, W.; Jia, R.; Yu, Y.; Zhang, B. Unveiling the Activity Origin of a Copper-based Electrocatalyst for Selective Nitrate Reduction to Ammonia. *Angew. Chem., Int. Ed.*, **2020**, *59*, 5350-5354.
- [16] Yao, Y.; Zhu, S.; Wang, H.; Li, H.; Shao, M. A Spectroscopic Study of Electrochemical Nitrogen and Nitrate Reduction on Rhodium Surfaces. *Angew. Chem., Int. Ed.*, **2020**, *59*, 10479-10483.
- [17] Li, J.; Zhan, G.; Yang, J.; et al. Efficient Ammonia Electrosynthesis from Nitrate on Strained Ruthenium Nanoclusters. *J. Am. Chem. Soc.*, **2020**, *142*, 7036-7046.
- [18] Zhao, Y.; Shi, R.; Bian, X.; et al. Ammonia Detection Methods in Photocatalytic and Electrocatalytic Experiments: How to Improve the Reliability of  $\text{NH}_3$  Production Rates? *Adv. Sci.*, **2019**, *6*, 1802109.
- [19] Li, L.; Tang, C.; Yao, D.; Zheng, Y.; Qiao, S.-Z. Electrochemical Nitrogen Reduction: Identification and Elimination of Contamination in Electrolyte. *ACS Energy Lett.*, **2019**, *4*, 2111-2116.
- [20] Carvalho, A. P.; Meireles, L. A.; Malcata, F. X. Rapid spectrophotometric determination of nitrates and nitrites in marine aqueous culture media. *Analisis*, **1998**, *26*, 347-351.
- [21] Liu, J.-X.; Richards, D.; Singh, N.; Goldsmith, B. R. Activity and Selectivity Trends in Electrocatalytic Nitrate Reduction on Transition Metals. *ACS Catal.*, **2019**, *9*, 7052-7064.
- [22] Wang, Z.; Young, S. D.; Goldsmith, B. R.; Singh, N. Increasing electrocatalytic nitrate reduction activity by controlling adsorption through PtRu alloying. *J. Catal.*, **2021**, *395*, 143-154.
- [23] Yang, J.; Sebastian, P.; Duca, M.; Hoogenboom, T.; Koper, M. T. pH dependence of the electroreduction of nitrate on Rh and Pt polycrystalline electrodes. *Chem. Commun.*, **2014**, *50*, 2148-2151.
- [24] Tucker, P. M.; Waite, M. J.; Hayden, B. E. Electrocatalytic reduction of nitrate on activated rhodium electrode surfaces. *J. Appl. Electrochem.*, **2004**, *34*, 781-796.
- [25] Taguchi, S.; Feliu, J. M. Kinetic study of nitrate reduction on Pt(110) electrode in perchloric acid solution. *Electrochim. Acta*, **2008**, *53*, 3626-3634.
- [26] Dima, G. E.; Beltramo, G. L.; Koper, M. T. M. Nitrate reduction on single-crystal platinum electrodes. *Electrochim. Acta*, **2005**, *50*, 4318-4326.
- [27] Chen, T.; Li, H.; Ma, H.; Koper, M. T. Surface modification of Pt(100) for electrocatalytic nitrate reduction to dinitrogen in alkaline solution. *Langmuir*, **2015**, *31*, 3277-3281.
- [28] Gootzen, J. F. E.; Peeters, P. G. J. M.; et al. The electrocatalytic reduction of  $\text{NO}_3^-$  on Pt, Pd and Pt + Pd electrodes activated with Ge. *J. Electroanal. Chem.*, **1997**, *434*, 171-183.
- [29] Zhu, J. Y.; Xue, Q.; Xue, Y. Y.; et al. Iridium Nanotubes as Bifunctional Electrocatalysts for Oxygen Evolution and Nitrate Reduction Reactions. *ACS Appl. Mater. Interfaces*, **2020**, *12*, 14064-14070.
- [30] Liu, H.; Park, J.; Chen, Y.; et al. Electrocatalytic Nitrate Reduction on Oxide-Derived Silver with Tunable Selectivity to Nitrite and Ammonia. *ACS Catal.*, **2021**, *11*, 8431-8442.
- [31] Fu, X.; Zhao, X.; Hu, X.; et al. Alternative route for electrochemical ammonia synthesis by reduction of nitrate on copper nanosheets. *Appl. Mater. Today*, **2020**, *19*, 100620.
- [32] Bae, S.; Gewirth, A. A. Differential reactivity of Cu(111) and Cu(100) during nitrate reduction in acid electrolyte. *Faraday Discuss.*, **2008**, *140*, 113-123.
- [33] Butcher, D. P.; Gewirth, A. A. Nitrate reduction pathways on Cu single crystal surfaces: effect of oxide and Cl. *Nano Energy*, **2016**, *29*, 457-465.
- [34] Zhou, G.; Yang, J. C. Initial Oxidation Kinetics of Cu(100), (110), and (111) Thin Films Investigated by in Situ Ultra-high-vacuum Transmission Electron Microscopy. *J. Mater. Res.*, **2005**, *20*, 1684-1694.
- [35] Lim, J.; Liu, C.-Y.; Park, J.; et al. Structure Sensitivity of Pd Facets for Enhanced Electrochemical Nitrate Reduction to Ammonia. *ACS Catal.*, **2021**, *11*, 7568-7577.

- [36] Li, L.; Tang, C.; Cui, X.; et al. Efficient Nitrogen Fixation to Ammonia through Integration of Plasma Oxidation with Electrocatalytic Reduction. *Angew. Chem., Int. Ed.*, **2021**, 60, 14131-14137.
- [37] Liu, S.; Wang, M.; Qian, T.; et al. Facilitating nitrogen accessibility to boron-rich covalent organic frameworks via electrochemical excitation for efficient nitrogen fixation. *Nat. Commun.*, **2019**, 10, 3898.
- [38] Tsvetkov, N.; Lu, Q.; Chen, Y.; Yildiz, B. Accelerated oxygen exchange kinetics on  $\text{Ni}_2\text{NiO}_4$  thin films with tensile strain along c-axis. *ACS Nano*, **2015**, 9, 1613-1621.
- [39] Yang, J.; Chen, X.; Yang, X.; Ying, J. Y. Stabilization and compressive strain effect of AuCu core on Pt shell for oxygen reduction reaction. *Energy Environ. Sci.*, **2012**, 5, 8976-8981.
- [40] Wang, Y.; Xu, A.; Wang, Z.; et al. Enhanced Nitrate-to-Ammonia Activity on Copper-Nickel Alloys via Tuning of Intermediate Adsorption. *J. Am. Chem. Soc.*, **2020**, 142, 5702-5708.
- [41] Li, Z.; Ji, S.; Liu, Y.; et al. Well-Defined Materials for Heterogeneous Catalysis: From Nanoparticles to Isolated Single-Atom Sites. *Chem. Rev.*, **2020**, 120, 623-682.
- [42] Chen, G.-F.; Yuan, Y.; Jiang, H.; et al. Electrochemical reduction of nitrate to ammonia via direct eight-electron transfer using a copper-molecular solid catalyst. *Nat. Energy*, **2020**, 5, 605-613.
- [43] Zhu, T.; Chen, Q.; Liao, P.; et al. Single-Atom Cu Catalysts for Enhanced Electrocatalytic Nitrate Reduction with Significant Alleviation of Nitrite Production. *Small*, **2020**, 16, e2004526.
- [44] Wu, Z. Y.; Karamad, M.; Yong, X.; et al. Electrochemical ammonia synthesis via nitrate reduction on Fe single atom catalyst. *Nat. Commun.*, **2021**, 12, 2870.
- [45] Li, P.; Jin, Z.; Fang, Z.; Yu, G. A single-site iron catalyst with preoccupied active centers that achieves selective ammonia electrosynthesis from nitrate. *Energy Environ. Sci.*, **2021**, 14, 3522-3531.
- [46] Niu, H.; Zhang, Z.; Wang, X.; et al. Theoretical Insights into the Mechanism of Selective Nitrate-to-Ammonia Electroreduction on Single-Atom Catalysts. *Adv. Funct. Mater.*, **2021**, 31, 2008533.
- [47] Jia, R.; Wang, Y.; Wang, C.; et al. Boosting Selective Nitrate Electroreduction to Ammonium by Constructing Oxygen Vacancies in  $\text{TiO}_2$ . *ACS Catal.*, **2020**, 10, 3533-3540.
- [48] Daiyan, R.; Tran-Phu, T.; Kumar, P.; et al. Nitrate reduction to ammonium: from CuO defect engineering to waste  $\text{NO}_x$ -to- $\text{NH}_3$  economic feasibility. *Energy Environ. Sci.*, **2021**, 14, 3588-3598.
- [49] Li, Y.; Go, Y. K.; Ooka, H.; et al. Enzyme Mimetic Active Intermediates for Nitrate Reduction in Neutral Aqueous Media. *Angew. Chem., Int. Ed.*, **2020**, 59, 9744-9750.
- [50] Chen, C.; Zhu, X.; Wen, X.; et al. Coupling  $\text{N}_2$  and  $\text{CO}_2$  in  $\text{H}_2\text{O}$  to synthesize urea under ambient conditions. *Nat. Chem.*, **2020**, 12, 717-724.